Effects of an impurity on the conductance and thermopower of a saddle-point-potential quantum point contact

C. S. Chu
Institute of Physics, National Chiao Tung University, Hsinchu 30050, Taiwan, Republic of China
and Department of Electrophysics, National Chiao Tung University, Hsinchu 30050, Taiwan, Republic Of China

Ming-Hui Chou
Department of Electrophysics, National Chiao Tung University, Hsinchu 30050, Taiwan, Republic Of China
(Received 18 May 1994; revised manuscript received 11 July 1994)

The conductance G and the thermopower S of a saddle-point-potential quantum point contact in the presence of a δ-potential impurity are calculated. For the case when an attractive impurity is located inside the quantum point contact, there are dips, peaks, and kinks in G. These structures can be found below and near the band bottom of some transverse subbands, respectively. The peaks in G give rise to double peaks in S and the dips in G give rise to a shift in the peak positions of S, towards a smaller chemical potential value. In addition, a broad dip in G is found to give rise to negative thermopower in regions between the peaks of S. For the case when an attractive impurity is located in the classical forbidden region for the electrons, we find in G the structures that correspond to resonance tunneling and resonance reflection. The corresponding S is found to show large and negative spikes. Our study shows that structures not so transparent in G manifest unequivocally in S, rendering S a very informative physical quantity to be measured.

I. INTRODUCTION

The quantum transport in quantum point contacts (QPC) has received a lot of attention, both theoretical[1] and experimental,[1] in recent years. These systems are electrostatically defined narrow constrictions connecting two high-mobility two-dimensional electron gas. The width W of a QPC is small ($W \approx \lambda_F$) enough to exhibit quantization effects, and the corresponding length L is short enough ($L \ll l$, the mean free path) to make possible the study of quantum ballistic transport. In the absence of defects and impurities, it is found experimentally[2,3] that the conductance G is quantized, in units of $2e^2/h$. However, this quantization in G is vulnerable to the presence of even one impurity in the constriction, according to recent theoretical[4–10] and experimental[11,12] studies. More specifically, theoretical studies show that the conductance G can exhibit dip structures just below the threshold of a transverse subband both in the case of a weak attractive short-range scatterer present in the constriction[5–7] and in the case of attractive long-range scatterers separated from the QPC by a spacer layer.[8] These dip structures in G are observed in recent experiments.[11,12] Thus dip structures in G can be used to distinguish an attractive scatterer from a repulsive scatterer but cannot be used to tell an in-plane scatterer from an off-plane scatterer.

Besides the conductance G, thermopower S is another physical property of QPC systems in which quantization effect manifests unequivocally. It was first shown theoretically by Streda[13] that in a narrow constriction the thermopower S exhibits peak structures. His calculation involved an ideal narrow constriction of which the longitudinal transmission coefficient through the constriction is a step function of energy, and he concluded that the peak values of S are quantized, given by $(k_B/e)\ln 2/(i+1/2)$. These peaks occur when the Fermi energy μ equals the threshold of the $(i+1)$th transverse subband, starting from $i=1$. Later theoretical studies[14,15] show similar oscillations in S except that these peak values are modified when the longitudinal transmission coefficient through the constriction is no longer a step function of energy, which corresponds to the case when the width of the constriction is changing, either adiabatically[14] or in a saddle-point-potential QPC.[15] The aforementioned quantum oscillations are demonstrated in recent experiments.[16,17] These peak features render S potentially very sensitive to the configuration of the QPC systems, especially when μ is in the vicinity of a transverse subband threshold. We expect that both G and S can be used to explore the configuration of QPC systems and that they play complementary roles in such regard. Hence we consider, in this paper, the effect of impurity on S in QPC systems.

Our purposes in this work are to study and to compare the effect of impurity on the thermopower S and the conductance G in QPC systems. The QPC is modeled by a saddle-point potential which is simple and quite realistic, giving no sharp corners and containing the essential features of the electrostatically induced QPC bottleneck.[18] The impurity is taken to be short range which, in the case of a saddle-point potential QPC, is appropriately described by a δ potential. The effect of the impurity location on G and S is studied by considering the impurity to be located in the central cross section of the QPC. Similar study has been carried out by Levinson *et al.*[9] for G using a confinement-potential Green's func-

tion method. In this work, we propose to apply another method, a mode-matching method, to the QPC systems. This method can be easily extended to other situations such as applying an external magnetic field to the QPC systems. In addition, new insights are obtained when our analysis includes both the cases for an impurity present *inside* and *outside* the QPC. An impurity is *outside* the QPC when it is located in the classical forbidden region for the electrons.

For an attractive impurity located *inside* the QPC, our results show dips and peaks in G which occur below and near the threshold of some transverse subbands, respectively. Sometimes, when μ is at the threshold of a transverse subband, the peaks are so small that they appear more like kinks in G. In addition, there is a resonance tunneling peak in G in the pinchoff region. The kinks in G give rise to double peaks in S and the dips in G give rise to a shift in the peak positions of S, towards a smaller chemical potential value. A broad dip in G is found to give negative thermopower, in regions between the peaks of S. The resonance tunneling in the pinchoff region results in S a large peak followed by a large negative dip. Our study shows that, near the threshold of a subband, S exhibits a relatively large double peak structure even in the case when G has only a small kink. This corroborates our intuition that S is sensitive to the QPC configuration near the threshold of a transverse subband.

For a not-too-weak attractive impurity located *outside* the QPC, our results show both additional peak and dip which corresponds to resonance tunneling and resonance reflection occurring *outside* the QPC. In such a regime, the thermopower S of the QPC deviates far from that of its impurity-free counterparts, exhibiting a large negative dip followed by a large positive spike. On the other hand, if the impurity *outside* the constriction is strongly attractive, the above resonant features of S disappear.

In Sec. II we develop a mode-matching method for the electron scattering in the saddle-point potential QPC. The thermopower is, within the Landauer multichannel approach,[19,20,13] related to the current transmission coefficients. In Sec. III we present some numerical examples to illustrate that S is very sensitive to the configuration of the QPC in the threshold region of a transverse subband. Finally, Sec. IV presents a conclusion.

II. IMPURITY SCATTERING IN SADDLE-POINT POTENTIAL

In this section, we consider a saddle-point potential QPC which connects two particle and energy reservoirs. The quantum transport phenomena are related to the quantum mechanical scattering in the QPC.[19,20] Incident electron in the nth transverse subband of the left reservoir is scattered in the QPC and gives rise to transmitted currents in all the propagating channels in the right reservoir. We stress that in the case of multichannel quantum scattering, we should be more specific when referring to transmission coefficient. There is transmission coefficient $|t_{nn'}|^2$ (Ref. 21) where $t_{nn'}$ is the coefficient appearing in the scattered wave function and is associated with the nth transmitted state. There is also a current transmission coefficient $T_{nn'}$ which is the ratio between the transmitted current in the nth channel and the incident current in the nth channel. These two transmission coefficients are different when n is different from n'. So far, this difference has not been emphasized enough and many papers use the term *transmission coefficient* when they actually are referring to current transmission coefficient.

In the following, the total transmitted current is expressed in terms of the current transmission coefficient $T_{nn'}$.[19,20] We take the left (right) reservoir to have chemical potential μ ($\mu - \Delta\mu$) and temperature $T + \Delta T$ (T). The total transmitted current, from the left to the right reservoir, is given by

$$J = -\frac{2e}{h}\int_{-\infty}^{\infty} dE\,[n_F(E,\mu,T+\Delta T) - n_F(E,\mu-\Delta\mu,T)]\sum_{n,n'} T_{nn'}\,, \tag{1}$$

where $n_F(E,\mu,T)$ is the Fermi-Dirac distribution function and $-e$ is the charge of an electron. In choosing the lower limit of the energy integration, we have assumed that $\mu - E_o \gg k_B T$, where E_o is the lowest electron energy in the reservoir.

Within the linear response regime, the conductance G is obtained from Eq. (1) by taking $\Delta T = 0$, and we have[20]

$$G = \frac{J}{\Delta V} = \frac{2e^2}{h}\int_{-\infty}^{\infty} dE\left(-\frac{dn_F}{dE}\right)\sum_{n,n'} T_{nn'}\,, \tag{2}$$

where $\Delta\mu = -e\Delta V$.

Similarly, within the linear response regime, the thermopower S is obtained from Eq. (1) by taking $J = 0$, such that[20]

$$S = -\frac{\Delta\mu}{e\Delta T} = \frac{k_B}{e}\frac{\displaystyle\int_{-\infty}^{\infty} dE\left(-\frac{dn_F}{dE}\right)\frac{E-\mu}{k_B T}\sum_{n,n'} T_{nn'}}{\displaystyle\int_{-\infty}^{\infty} dE\left(-\frac{dn_F}{dE}\right)\sum_{n,n'} T_{nn'}}. \tag{3}$$

The current transmission coefficients $T_{nn'}$ depend on the configuration of the QPC. In the following, we consider a saddle-point potential $V_{sp}(x,y)$, given by

$$V_{sp}(x,y) = U_o - U_x x^2 + U_y y^2, \tag{4}$$

where the electrostatic potential at the saddle U_o is taken to be zero. An impurity located in the central cross section of the saddle-point potential, with the impurity potential $V_{\rm imp}$ given by

$$V_{\rm imp}(x,y) = V_o\,\delta(x)\,\delta(y-y_o). \tag{5}$$

We note, in passing, that the numerical results obtained using a δ potential $V_{\rm imp}(x,y)$, as in Eq. (5), are essentially the same as using a finite-but-short-range potential for $V_{\rm imp}$, as long as the potential range is shorter than all other relevant length scales.[9] In such cases, the constant V_o in Eq. (5) is given by

$$V_o = \int V_{\rm imp}(x,y)dxdy.$$

Choosing the energy unit $E^* = \hbar^2 k_F^2/2m$ and the length unit $a^* = 1/k_F$, where k_F is a typical Fermi wave vector of the reservoir, the two-dimensional Schrödinger equation becomes

$$\left[-\nabla^2 - \omega_x^2 x^2 + \omega_y^2 y^2 + v_o\,\delta(x)\,\delta(y-y_o)\right]\Psi(x,y) = E\Psi(x,y). \quad (6)$$

Here, $\omega_x = \sqrt{2mU_x}/\hbar k_F^2$, $\omega_y = \sqrt{2mU_y}/\hbar k_F^2$, and $v_o = 2mV_o/\hbar^2$. The configuration of the QPC is characterized by the dimensionless parameters ω_x, ω_y, v_o, and y_o. In particular, the ratio $(\omega_y/\omega_x) \equiv L/W$, where W (L) is the effective width (length) of the QPC.

The unperturbed transverse motion is quantized into subbands, with energy $(2n+1)\omega_y$ and normalized wave function

$$\phi_n(y) = \left(\frac{\omega_y}{\pi}\right)^{1/4} \frac{1}{\sqrt{2^n\, n!}} H_n(\sqrt{\omega_y}\, y)\, \exp\left(\frac{-\omega_y\, y^2}{2}\right), \quad (7)$$

where H_n is the Hermite polynomial and n starts from zero.

The unperturbed wave function $\psi_n(x)$ along the QPC for an electron in the nth subband satisfies the equation

$$\left[\frac{\partial^2}{\partial x^2} + \omega_x^2 x^2 + \epsilon_n\right]\psi_n(x) = 0, \quad (8)$$

where $\epsilon_n = E - (2n+1)\omega_y$ is the energy for the motion along x direction. The dependence of $\psi_n(x)$ on ϵ_n is implied. For every value of ϵ_n, there are two $\psi_n(x)$'s, given by[22]

$$\psi_{ne}(x) = \exp\left(\frac{-i\omega_x x^2}{2}\right) M\left(\frac{1}{4} + i\frac{\epsilon_n}{4\omega_x}, \frac{1}{2}, i\omega_x x^2\right) \quad (9)$$

and

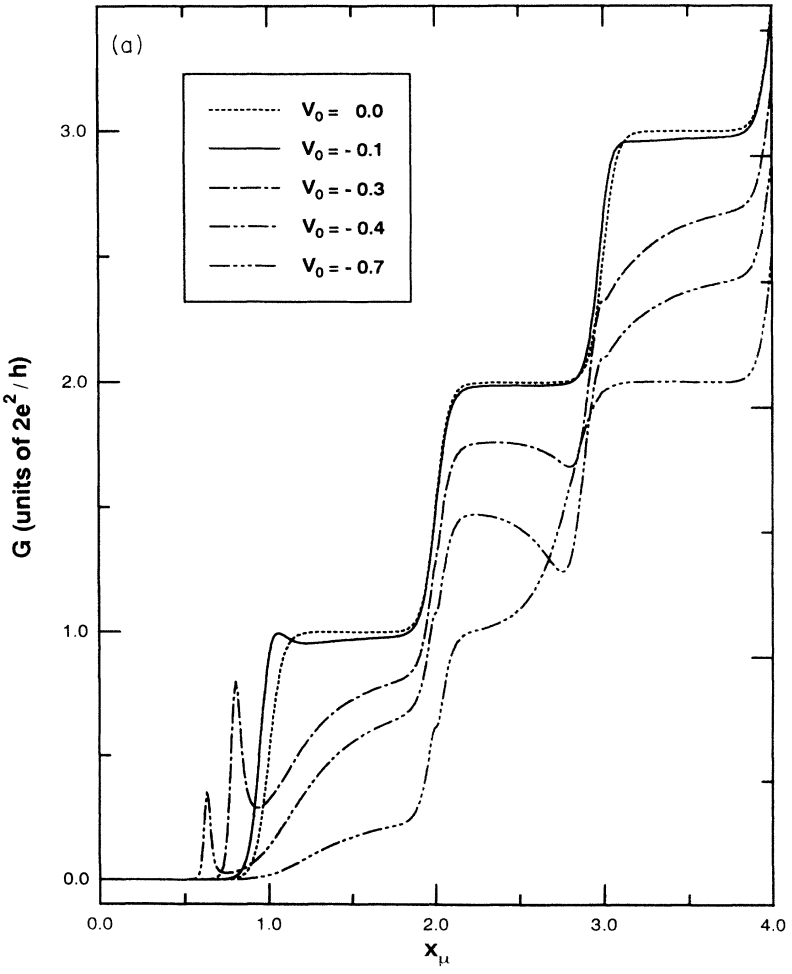

FIG. 1. (a) Conductance G of the QPC as a function of x_μ. The $v_o = 0.0$ case corresponds to an ideal QPC. Four other impurity strengths: $v_o = -0.1, -0.3, -0.4$, and -0.7 are shown. The impurity is located at the center of the QPC. (b) Thermopower S of the QPC as a function of x_μ for the same QPC configuration as in (a). The inset figure shows detail S structures near $x_\mu = 2$.

$$\psi_{no}(x) = x\sqrt{\omega_x}\exp\left(\frac{-i\omega_x x^2}{2}\right) \times M\left(\frac{3}{4} + i\frac{\epsilon_n}{4\omega_x}, \frac{3}{2}, i\omega_x x^2\right). \quad (10)$$

Here, ψ_{ne} (ψ_{no}) is an even (odd) function of x and $M(a,b,z)$ is Kummer's function.[23]

Using ψ_{ne} and ψ_{no}, we construct a state $\psi_{n,\mathrm{in}}(x)$ [$\psi_{n,\mathrm{ref}}(x)$] which has only positive (negative) current density in the asymptotic region ($x \to -\infty$). Similarly, we construct a state $\psi_{n,\mathrm{out}}$ which has only positive current density in the asymptotic region $x \to +\infty$. The results are

$$\begin{aligned}\psi_{n,\mathrm{in}}(x) &= \psi_{no}(x) + \alpha_n \psi_{ne}(x),\\ \psi_{n,\mathrm{out}}(x) &= \psi_{no}(x) + \beta_n \psi_{ne}(x),\\ \psi_{n,\mathrm{ref}}(x) &= \psi_{no}(x) + \gamma_n \psi_{ne}(x),\end{aligned} \quad (11)$$

where

$$\alpha_n = \frac{1-i}{4\pi}\left[\cosh\left(\frac{\pi\epsilon_n}{4\omega_x}\right) - i\sinh\left(\frac{\pi\epsilon_n}{4\omega_x}\right)\right] \times \left|\Gamma\left(\frac{1}{4} + i\frac{\epsilon_n}{4\omega_x}\right)\right|^2, \quad (12)$$

and $\gamma_n = -\beta_n = \alpha_n^*$.

With an impurity located at $(x,y) = (0, y_o)$, the scattering wave function of an nth subband electron with total energy E and incident from the left-hand side can be written in the form

$$\Psi_n^+(x,y) = \begin{cases} \phi_n(y)\,\psi_{n,\mathrm{in}}(x) + \sum_{m'} r_{m'n}\,\phi_{m'}(y)\,\psi_{m',\mathrm{ref}}(x)\ , & x < 0\ , \\ \sum_{n'} t_{n'n}\,\phi_{n'}(y)\,\psi_{n',\mathrm{out}}(x)\ , & x > 0\ . \end{cases} \quad (13)$$

Matching the wave function Ψ_n^+ at $x = 0$ and integrating the Schrödinger equation across $x = 0$ leads to two matrix equations

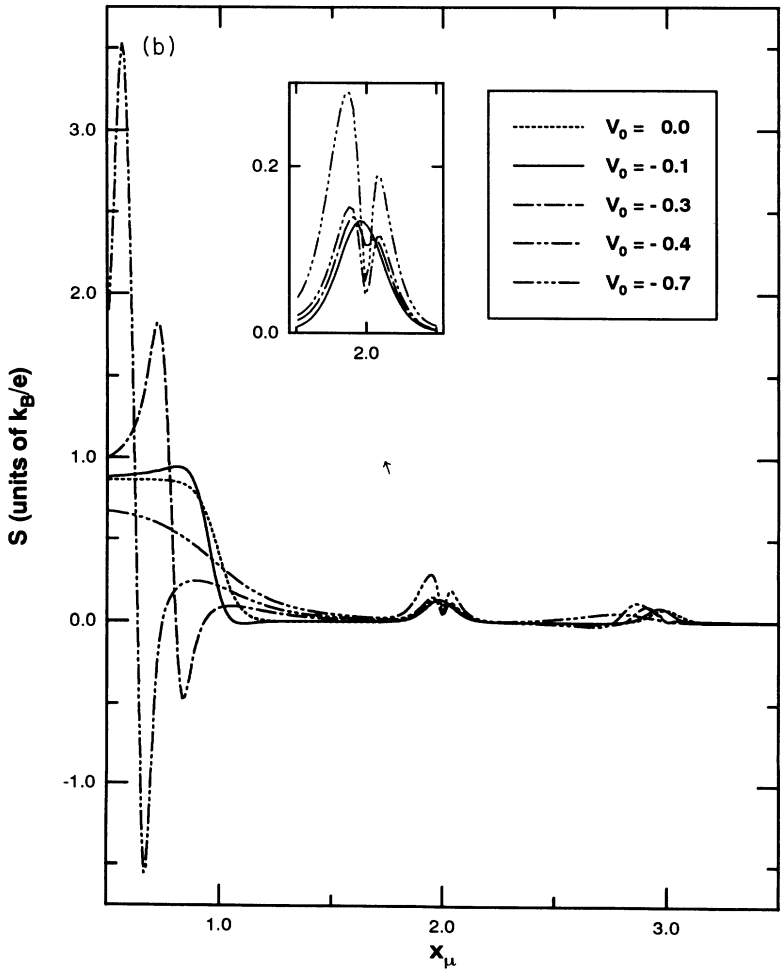

FIG. 1. (*Continued*).

$$\boldsymbol{\alpha} + \boldsymbol{\gamma}\,\mathbf{R} = \boldsymbol{\beta}\,\mathbf{T}, \tag{14}$$

$$\mathbf{1} + \mathbf{R} = \mathbf{J}\,\mathbf{T}, \tag{15}$$

where

$$\begin{aligned}
(\boldsymbol{\alpha})_{mn} &= \alpha_n\,\delta_{mn},\\
(\boldsymbol{\beta})_{mn} &= \beta_n\,\delta_{mn},\\
(\boldsymbol{\gamma})_{mn} &= \gamma_n\,\delta_{mn},\\
(\mathbf{R})_{mn} &= r_{mn},\\
(\mathbf{T})_{mn} &= t_{mn},\\
(\mathbf{J})_{mn} &= \delta_{mn} - \frac{2v_o}{\sqrt{\omega_x}}\,\phi_m(y_o)\,\phi_n(y_o)\,\beta_n\ .
\end{aligned} \tag{16}$$

From Eq. (14) and Eq. (15), we obtain the transmission coefficients t_{mn}, which is the matrix element of $\mathbf{T}$ and is given by

$$\mathbf{T} = (\boldsymbol{\beta} - \boldsymbol{\gamma}\,\mathbf{J})^{-1}(\boldsymbol{\alpha} - \boldsymbol{\gamma}). \tag{17}$$

The matrix $\mathbf{T}$ is symmetric because both $(\boldsymbol{\beta} - \boldsymbol{\gamma}\,\mathbf{J})$ and $(\boldsymbol{\alpha} - \boldsymbol{\gamma})$ are symmetric. In deriving the above matrix equations, we have used the relations $\psi_{ne}(0) = 1$, $\psi'_{ne}(0) = \psi_{no}(0) = 0$, and $\psi'_{no}(0) = \sqrt{\omega_x}$, where the *prime* means derivative with respect to x. It is straightforward to show from Eq. (17) that, in the case of no impurity ($v_o = 0$), $t_{nn'} = \delta_{nn'}\,[1 + \exp(-\pi\epsilon_n/\omega_x)]^{-1}$, which is the well-known result for a perfect saddle-point potential.[18]

The incident current $J_{n,\mathrm{inc}}$ is given by

$$J_{n,\mathrm{inc}} = \lim_{x\to-\infty} C_o(\alpha_n\,\psi_{ne} + \psi_{no})\,\frac{\partial}{\partial x}(\alpha_n\,\psi_{ne} + \psi_{no})^*, \tag{18}$$

and the transmitted current $J_{n',\mathrm{tran}}$ in the nth channel is given by

$$\begin{aligned}
J_{n',\mathrm{tran}} = \lim_{x\to\infty} C_o \mid t_{n'n} \mid^2 (\beta_{n'}\,\psi_{n'e} + \psi_{n'o})\\
\times \frac{\partial}{\partial x}(\beta_{n'}\,\psi_{n'e} + \psi_{n'o})^*\ .
\end{aligned} \tag{19}$$

Here, C_o is a dimensionless constant.

The current transmission coefficient $T_{nn'}$ is given by

$$T_{nn'} = \frac{J_{n',\mathrm{tran}}}{J_{n,\mathrm{inc}}}. \tag{20}$$

Finally, substituting Eqs. (18) and (19) into Eq. (20), and taking the required asymptotic limit, we have

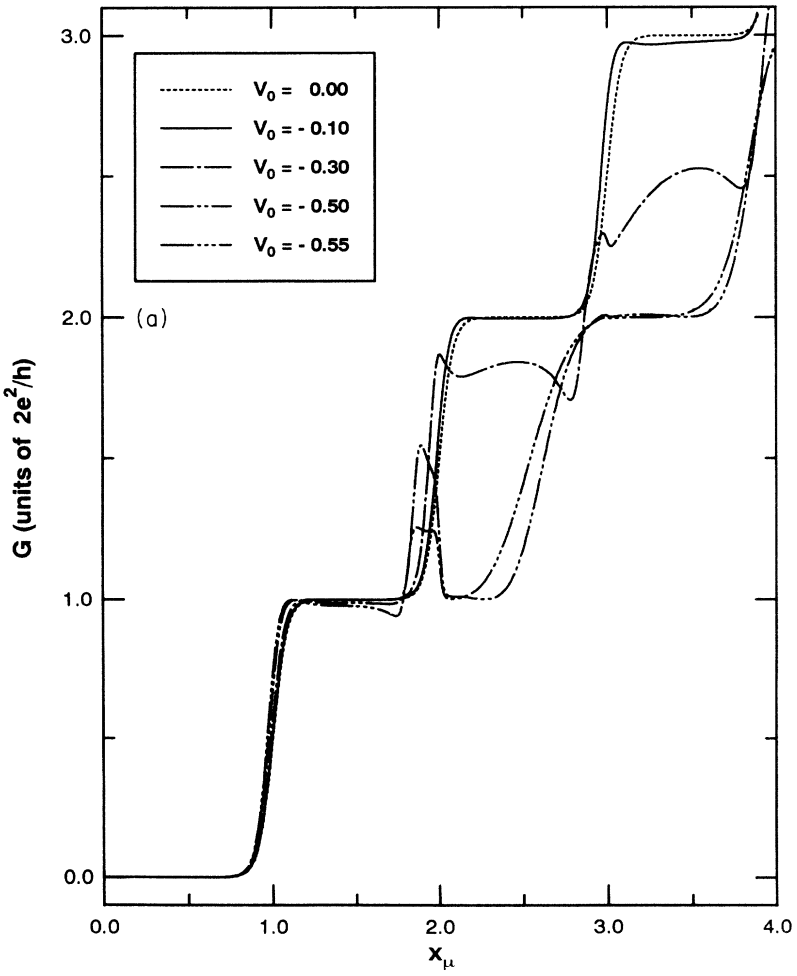

FIG. 2. (a) Conductance G of the QPC as a function of x_μ. The impurity is *at the edge* of the QPC when $x_\mu = 2.1$. The dotted curve corresponds to the ideal QPC results and four other impurity strengths are shown. (b) Thermopower S of the QPC as a function of x_μ. The configuration is the same as in (a).

$$T_{nn'} = |t_{n'n}|^2 \exp\left[(n-n')\frac{\pi}{2}\frac{\omega_y}{\omega_x}\right] \times \frac{\left|\Gamma\left(\frac{3}{4}+i\frac{\epsilon_n}{4\omega_x}\right)\right|^2 \cosh\left(\frac{\pi\epsilon_n}{2\omega_x}\right)}{\left|\Gamma\left(\frac{3}{4}+i\frac{\epsilon_{n'}}{4\omega_x}\right)\right|^2 \cosh\left(\frac{\pi\epsilon_{n'}}{2\omega_x}\right)} . \quad (21)$$

In the case when there is no impurity, it is obvious that $t_{nn'}$ is diagonal and that $T_{nn'} = |t_{nn'}|^2$.

III. NUMERICAL EXAMPLES

In this section, we present in three different situations the G and S of a QPC as a function of the chemical potential μ of the reservoir. The effective width of the QPC is increased as μ increases. In the first situation, an attractive impurity is fixed in its location, closer to the symmetry axis, such that the impurity is always *inside* the QPC. In the second situation, an attractive impurity is, again, fixed in its position but is at a greater distance from the symmetry axis such that it is *outside* the QPC in the lower μ regime and is *inside* the system in the higher μ regime. The effect of the impurity strength is also examined in the above two situations. Finally, in the third situation, the strength of the impurity is fixed while its transverse location is changing.

We take the QPC to be that in a high-mobility GaAs-$Al_xGa_{1-x}As$ with typical electron density $n \sim 2.5 \times 10^{11}$ cm^{-2}, $m^* = 0.067\, m_e$, and $\lambda_F = 500$ Å. Thus our choice of length scale $a^* = k_F^{-1} = 79.6$ Å, and energy scale $E^* = \hbar^2 k_F^2/2m^* = 9$ meV $= 104$ K. In all the following numerical examples, we have chosen $k_BT = 0.01$ ($T \sim 1$ K), $\omega_x = 0.125$, and $\omega_y = 0.5$. With such choice of parameters, the QPC's effective length to width ratio $L/W = 4$. In the following numerical examples, the impurity potentials v_o were, in fact, rescaled and became $v_o/\sqrt{\omega_x}$.

In Figs. 1(a) and 1(b), we plot the variation of G and S, respectively, of a QPC as a function of the chemical potential μ. For convenient purposes, the abscissa is given by x_μ

$$x_\mu = \frac{1}{2}\left(\frac{\mu}{\omega_y}+1\right), \quad (22)$$

which truncated integer value is the number of propagating channels below μ. The effective half-width of the QPC is given by $y \approx \sqrt{(2x_\mu - 1)/\omega_y}$ for $x_\mu \geq 0.5$. An attractive impurity is located at $(x_o, y_o) = (0,0)$. Our results include cases of five impurity strengths: $v_o =$

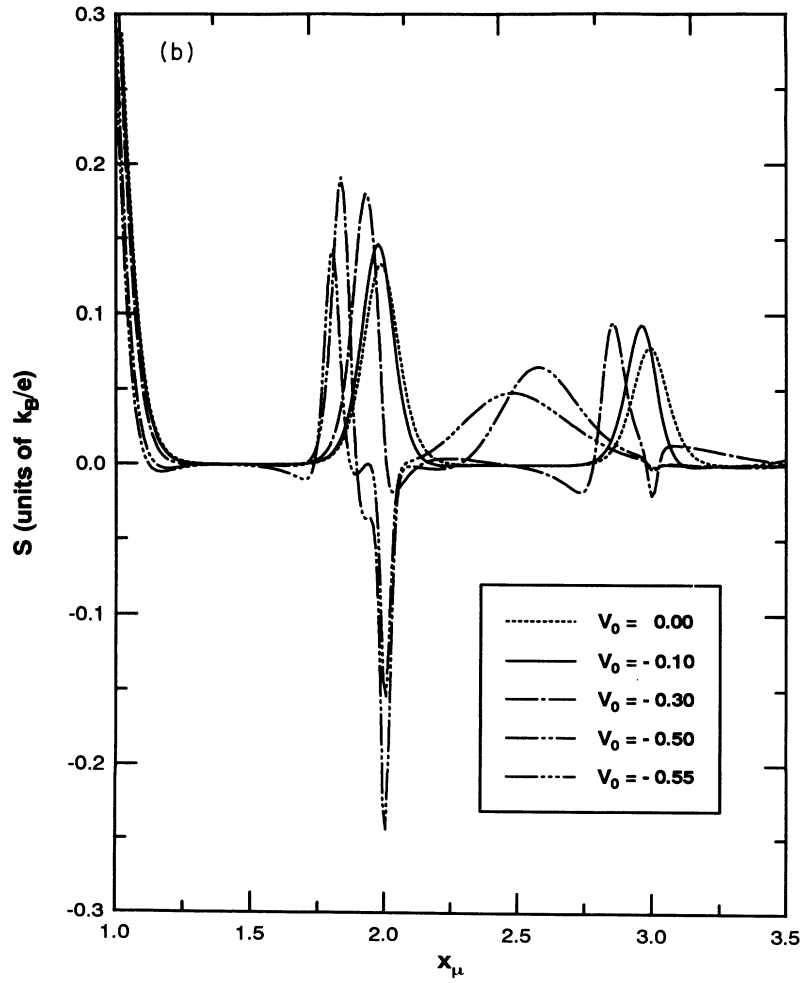

FIG. 2. (*Continued*).

$0.0, -0.1, -0.3, -0.4$, and -0.7. Except in the pinchoff region ($x_\mu < 1$), the impurity remains *inside* the QPC.

There is, in the pinchoff region, no propagating channel in the QPC so that transmission occurs only through tunneling which gives rise to a peak in G, as is shown in Fig. 1(a). For a more attractive impurity, this peak in G occurs at a lower x_μ and with a lower peak height. These features are consistent with the interpretation of such a peak in terms of resonant tunneling transmission. In the case of a more attractive impurity, the resonant peak in G occurs at a lower x_μ because μ has to line up with a lower quasibound state. On the other hand, in the saddle-point potential configuration, the effective tunneling distance is increased, rendering the peak height in G to be lowered. For an even more attractive impurity, such as $v_o \geq -0.7$ in Fig. 1(a), there is no resonant peak because the impurity quasibound state is too deep to allow resonant tunneling to occur. For the case of thermopower, in this pinchoff region, the resonant tunneling gives rise to a pair of positive peak and negative dip structures, with the peak locating on the lower x_μ side. We find that this peak-dip structure can be understood qualitatively by noting firstly in Eq. (3) that S is zero when $\sum_{n,n'} T_{nn'}$ is a constant near μ and, secondly, that if $\sum_{n,n'} T_{nn'}$ were to depend linearly on energy near μ, S would be proportional to the slope of $\sum_{n,n'} T_{nn'}$. In the low temperature regime, as we consider here, we have $\sum_{n,n'} T_{nn'} \sim G$, and the peak-dip structure in S is found to reflect qualitatively the slope of the peak in G. With this insight, we point out in particular that for the cases $v_o = -0.3$, and -0.4, the former case has a larger peak in G but a smaller peak-dip magnitude. This is related to the fact that the former peak has a slower rate of rise and drop. This result demonstrates clearly the *G-profile-sensitive* feature of S in the low temperature regime.

In the region when there are propagating channels, there are dip structures in G just below $x_\mu = 3$ for the cases $v_o = -0.3$ *and* -0.4. Following a dip structure, on the larger x_μ side, G rises more rapidly and has a greater slope than the case for an ideal QPC. Thus, applying our *G-profile-sensitive* analysis for S, the effect of the dip structure in G is to give rise to a larger peak as well as a shift in the peak location of S towards a lower x_μ value. This feature is demonstrated in Fig. 1(b) near $x_\mu = 3$. Furthermore, a broad dip, such as the case for $v_o = -0.4$, gives rise to negative S in the region when x_μ is between 2 and 3. Besides dip structure in G, there is a kink in G at $x_\mu = 2$. Similar structures have been found by Levinson *et al.* [9] These kinks in G are not found in narrow constrictions of which the confinement potentials are

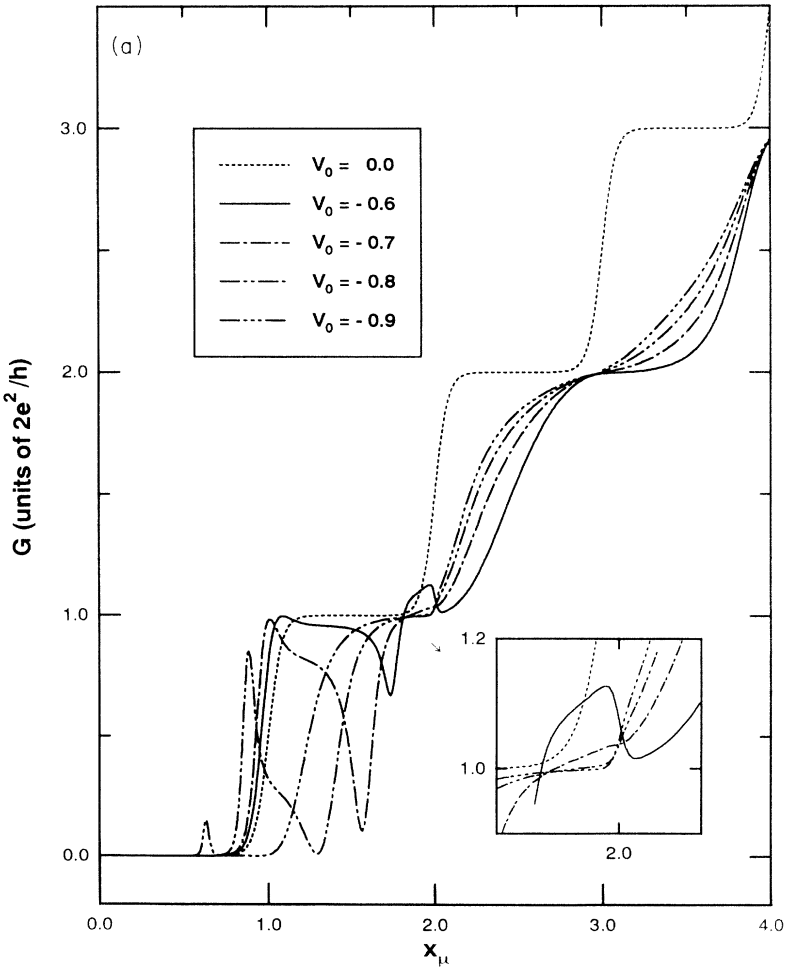

FIG. 3. (a) G vs x_μ. The location of the impurity is the same as in 2(a). The figure shows that a more attractive impurity gives rise to resonant reflection and transmission when it is still *outside* ($x_\mu < 2.1$) the QPC. (b) S vs x_μ. Same configuration as in (a).

independent of the longitudinal coordinates. The kink in G is shown, in Fig. 1(b), to give rise to a double-peak structure in S. This can be explained with our *G-profile-sensitive* analysis. We point out that for $v_o = -0.7$, the kink in G is barely recognizable while the corresponding double peak in S is quite spectacular, with the higher peak height almost double that of the ideal QPC.

Figures 2(a), 2(b), 3(a), and 3(b) show the G and S, respectively, for the case when the impurity is located at $y_o = 2.5$. The impurity strength varies from $v_o = 0.0$ to $v_o = -0.9$. As the chemical potential μ increases, the effective width of the QPC is increasing and the impurity location changes from effectively *outside* to *inside* the QPC. In particular, the impurity is *at the edge* of the QPC when $x_\mu = (\omega_y y_o^2 + 1)/2$. We take $\omega_y = 0.5$ so that the critical x_μ is about 2.1. One main purpose of plotting Figs. 2(a) and 2(b) is to show that, for a not-so-attractive impurity ($v_o \leq -0.55$), the impurity effect only becomes evident when it is *effectively inside* the QPC. Figures 3(a) and 3(b) show, however, that a more attractive impurity has its effect felt even when it is still *effectively outside* the QPC.

From Fig. 2(a), we see that for $v_o = -0.1$ and $v_o = -0.3$, a significant effect of the impurity comes in when $x_\mu \geq 2.1$. This is reasonable because the impurity affects the transport when it is effectively *inside* the QPC. The latter impurity gives a dip and a small peak in G near $x_\mu = 3$. The dip-and-peak structure in G ($x_\mu \sim 3$ and $v_o = -0.3$) gives rise in S to a positive peak in between two negative dips, as shown in Fig. 2(b). As shown in Figs. 2(a) and 2(b), the G plateaus as well as the dip structures in region $x_\mu \geq 2$ are destroyed when the impurity becomes more attractive. Thus the rising in G for $x_\mu \approx 3$ becomes less abrupt. The corresponding feature in S is a gradual shift in the peak of S, away from the ideal QPC peak at $x_\mu = 3$ and towards a smaller x_μ value. Following the shifting of peak positions in S, these peaks are broadened and their peak height lowered. In addition, there is a peak in G, near $x_\mu = 2$, which is associated with resonance tunneling occurring near the edge of the QPC. This peak becomes more pronounced for a more attractive impurity and the corresponding S exhibits a peak followed by a large negative spike. For the case $v_o = -0.5$, the magnitude of the negative S spike is even greater than the magnitude of the ideal peak in S. This is a signature of a pronounced peak in G.

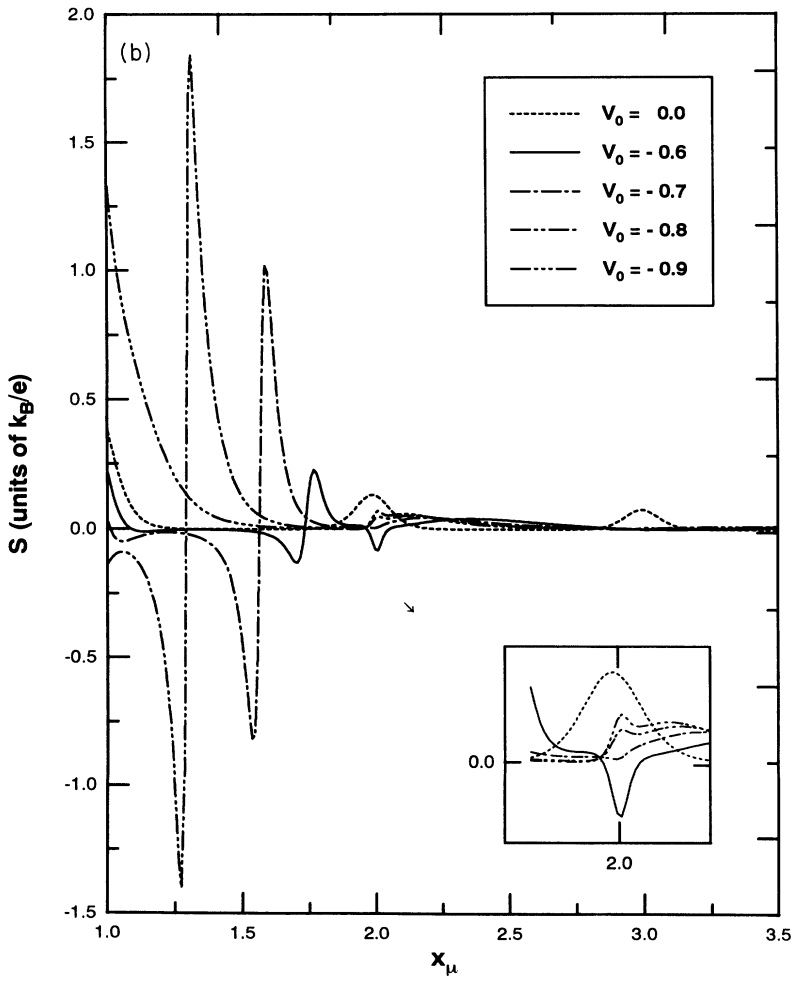

FIG. 3. (*Continued*).

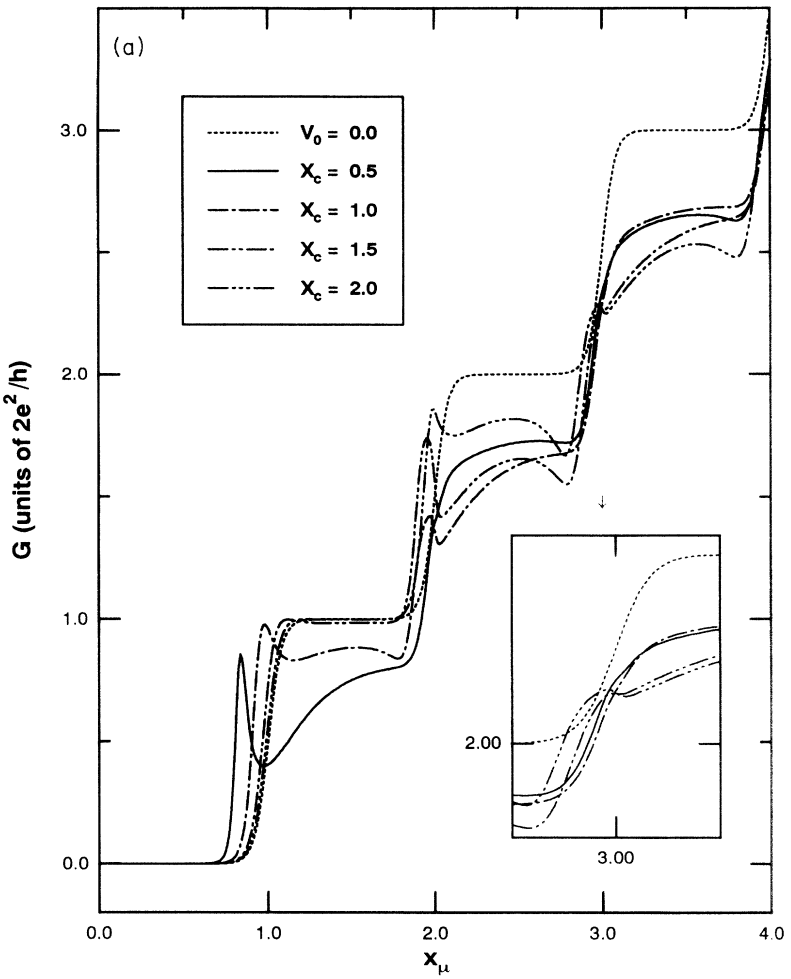

FIG. 4. (a) G vs x_μ. The impurity potential $v_o = -0.3$, the ideal QPC curve is given by the dotted curve. Four impurity positions are shown. The impurity is *at the edge* of the QPC when $x_c = x_\mu$. (b) S vs x_μ. Same configuration as in (a).

As the impurity becomes even more attractive, as shown in Figs. 3(a) and 3(b), new G and S structures are developed in the region $x_\mu \leq 2$, which corresponds to resonant reflection and resonant transmission when the impurity is quite *outside* the QPC. Corresponding to the resonant reflection dip in G, there is a large negative spike following by a large positive peak structure in S. Note, in particular, that the magnitudes of both the spike and the peak can be up to five to six times that of the ideal S peak at $x_\mu = 1$. This demonstrates that S is very sensitive to resonant processes in the QPC systems.

Finally, in Figs. 4(a) and 4(b), we plot G and S for a $v_o = -0.3$ impurity in various positions: $x_c = 0.5, 1.0, 1.5$, and 2.0. The impurity is *at the edge* of the QPC when $x_\mu = x_c$. From the results in previous figures, we see that this impurity is a weak attractive scatterer. In the pinchoff region, the $x_c = 0.5$ and 1.0 impurities give rise to a resonant tunneling peak in G. The $x_c = 2.0$ impurity gives rise to a peak in G due to resonant tunneling *outside* the QPC. However, it is interesting to note that the $x_c = 1.0, 1.5$ impurities contribute to peaks in G near $x_\mu = 2$ where the impurities are already *inside* the QPC. Our results show that the impurity with $x_c = 2.0$ gives rise to a larger G peak at $x_\mu = 2$ while it gives rise only to a kink in G at integer $x_\mu = 3$. The corresponding structure in S for this peak consists of a negative dip, as shown in Fig. 4(b).

IV. CONCLUSION

A mode-matching technique has been applied to study the effect of an impurity on the conductance and the thermopower of a saddle-point-potential QPC. Our analysis demonstrates the correlation between the conductance and the thermopower in the low temperature regime. The correlation is established qualitatively using a *G-profile-sensitive* analysis. We show that S is very sensitive to the impurity near the threshold of a transverse subband. In fact, our results show that S is closely related to the slope of G. At integral x_μ values, kinks in G which are not so transparent can give rise to large double peaks in S. Large negative spikes in S arise due to the presence of sharper peaks and dips in G. Thus S is sensitive to the resonant tunneling peak and resonant

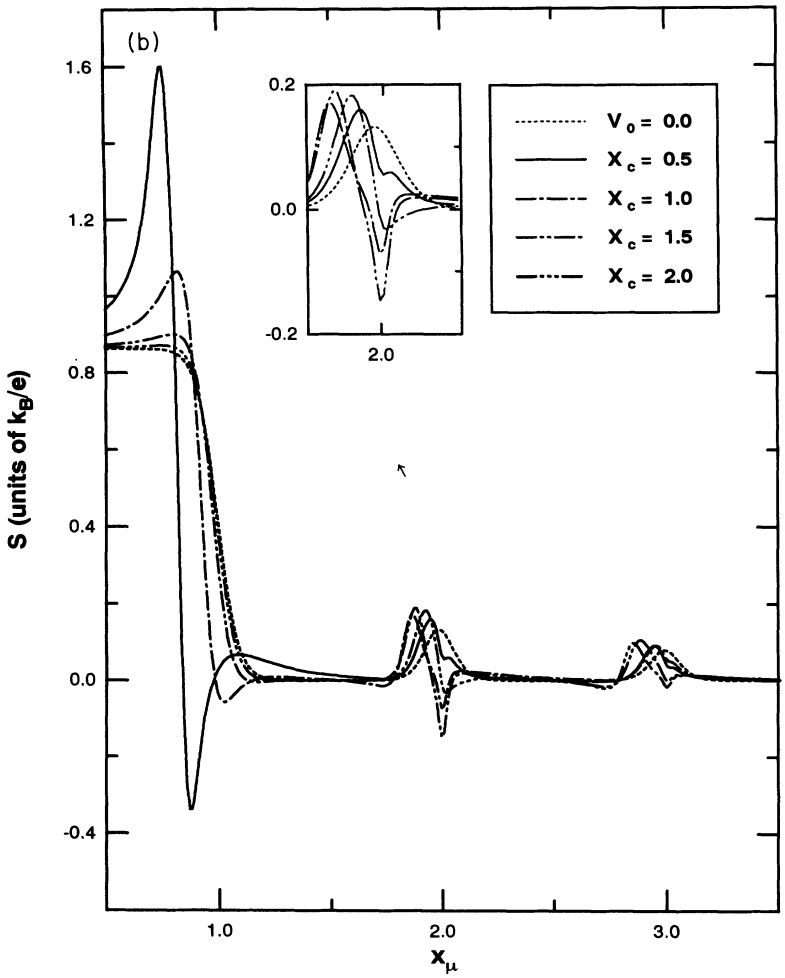

FIG. 4. (*Continued*).

reflection dip in G.

Besides, we have studied the cases when the impurity is *outside* and *inside* the QPC and have demonstrated the resonant tunneling and the resonant reflection occurring *outside* the QPC. Our results show in detail the effect on S and G when a short-range impurity is around the *edge* of the QPC. Finally, this study shows that both G and S can be used to explore the configuration of QPC systems and that they play complementary roles in such regard.

ACKNOWLEDGMENTS

This work was partially supported by the National Science Council of the Republic of China through Contract No. NSC82-0208-M-009-062.

[1] C. W. J. Beenakker and H. van Houten, in *Solid State Physics*, edited by H. Ehrenreich and D. Turnbull (Academic, New York, 1991), Vol. 44, p. 1.
[2] B. J. van Wees, H. van Houten, C. W. J. Beenakker, J. G. Williamson, L. P. Kouwenhoven, D. van der Marel, and C. T. Foxon, Phys. Rev. Lett. **60**, 848 (1988).
[3] D. A. Wharam, T. J. Thornton, R. Newbury, M. Pepper, H. Ahmed, J. E. F. Frost, D. G. Hasko, D. C. Peacock, D. A. Ritchie, and G. A. C. Jones, J. Phys. C **21**, L209 (1988).
[4] D. van Marel and E. G. Haanapel, Phys. Rev. B **39**, 7811 (1989).
[5] C. S. Chu and R. S. Sorbello, Phys. Rev. B **40**, 5941 (1989).
[6] P. Bagwell, Phys. Rev. B **41**, 10 354 (1990).
[7] E. Tekman and S. Ciraci, Phys. Rev. B **43**, 7145 (1991).
[8] J. A. Nixon, J. H. Davies, and H. U. Baranger, Phys. Rev. B **43**, 12 638 (1991).
[9] Y. B. Levinson, M. I. Lubin, and E. V. Sukhorukov, Phys. Rev. B **45**, 11 936 (1992).
[10] Y. Takagaki and D. K. Ferry, Phys. Rev. B **46**, 15218 (1992).
[11] J. Faist, P. Guéret, and H. Rothuizen, Phys. Rev. B **42**, 3217 (1990).
[12] C. C. Eugster, J. A. del Alamo, M. R. Melloch, and M. J. Rooks, Phys. Rev. B **46**, 10 146 (1992).

[13] P. Streda, J. Phys. Condens. Matter **1**, 1025 (1989).
[14] C. R. Proetto, Phys. Rev. B **44**, 9096 (1991).
[15] Y. Okuyama and N. Tokuda, Phys. Rev. B **46**, 2610 (1992).
[16] L. W. Molenkamp, H. van Houten, C. W. J. Beenakker, R. Eppenga, and C. T. Foxon, Phys. Rev. Lett. **65**, 1052 (1990).
[17] L. W. Molenkamp, Th. Gravier, H. van Houten, O. J. A. Buijk, M. A. A. Mabesoone, and C. T. Foxon, Phys. Rev. Lett. **68**, 3765 (1992).
[18] M. Büttiker, Phys. Rev. B **41**, 7906 (1990).
[19] M. Büttiker, Y. Imry, R. Landauer, and S. Pinhas, Phys. Rev. B **31**, 6207 (1985).
[20] U. Sivan and Y. Imry, Phys. Rev. B **33**, 551 (1986).
[21] This definition of transmission coefficient can be found in a standard quantum mechanics textbook such as L. I. Schiff, *Quantum Mechanics* (McGraw-Hill, New York, 1971), p. 103.
[22] H. A. Fertig and B. I. Halperin, Phys. Rev. B **36**, 7969 (1987).
[23] M. Abramowitz and I. A. Stegun, *Handbook of Mathematical Functions* (Dover, New York, 1972), p. 504.